Contents lists available at SCCE

Journal of Soft Computing in Civil Engineering

Journal homepage: www.jsoftcivil.com

Application of Contourlet Transform in Damage Localization and Severity Assessment of Prestressed Concrete Slabs

H. Jahangir[1], M. Khatibinia[2*], M. Kavousi[3]

1. Assistant Professor, Department of Civil Engineering, University of Birjand, Birjand, Iran
2. Associate Professor, Department of Civil Engineering, University of Birjand, Birjand, Iran
3. M.Sc. in Structural Engineering, Civil Engineering Department, Hormozan University of Birjand, Birjand, Iran
Corresponding author: *m.khatibinia@birjand.ac.ir*

https://doi.org/10.22115/SCCE.2021.282138.1301

ARTICLE INFO

Article history:
Received: 19 April 2021
Revised: 19 June 2021
Accepted: 12 July 2021

Keywords:
Contourlet transform;
Modal data;
Damage localization;
Damage severity assessment;
Prestressed concrete slab.

ABSTRACT

In this paper, the location and severity of damages in prestressed concrete slabs are assessed using the contourlet transform as a novel signal processing method. To achieve this goal, the numerical models of prestressed concrete slabs were built based on the experimental specimens reported in the previous research works. Then, the single, double, and triple damage scenarios with various geometric shapes (transverse, longitudinal, inclined, and curved slots) at different positions (middle and corners) were created in the models. To assess the severity of damages, the depth of slots was taken constant in the single and double damage scenarios and assumed variable in the triple ones. The vibration mode shapes together with their corresponding curvatures were obtained using the modal analysis. The contourlet transform coefficients of modal curvatures in two states of damaged and undamaged models were taken as the inputs for the proposed damage index. The results show that the proposed damage index has well identified the severity of triple damage scenarios in addition to detecting the location of different single and double damages at the middle and in the vicinity of corner and supports of the prestressed concrete slab models. Furthermore, the proposed damage index has the highest sensitivity rate to damage scenarios with geometric shapes of inclined, curved, transverse, and longitudinal slot, respectively.

How to cite this article: Jahangir H, Khatibinia M, Kavousi M. Application of contourlet transform in damage localization and severity assessment of prestressed concrete slabs. J Soft Comput Civ Eng 2021;5(2):39-67. https://doi.org/10.22115/scce.2021.282138.1301.

1. Introduction

The high cost of construction and the importance of some of these structures have obliged researchers to look after methods for early detection of damages at the initial stages [1]. By the right and early identification of damaged elements in the structure and by reinforcing via fibers [2–6] and smart materials [7,8], or strengthening them with different kinds of composites [9–14], one could schedule the operation and maintenance of structures.

Structural health monitoring (SHM) is a set of processes including data acquisition, data processing, extraction of properties sensitive to damage, and decision making for damage localization and determining the severity. A large number of damage identification methods are based on the direct analysis of vibration responses in the time domain [15]. As the raw data obtained from the sensors are normally nonlinear and highly complex, their assessment requires efficient tools like soft computing techniques [16–19] or signal processing methods. Among various methods of signal processing, the wavelet transform is a novel method that is capable of local signal analysis at different times and frequencies [20–22]. The wavelet transform of a signal could detect some of its hidden aspects like discontinuities and fractured points. Hence, in some research work, it is applied to the vibration responses in the time domain to detect damages in structures [23–27]. In some cases, the data obtained from the installed sensors on the structure are investigated in the frequency domain and in the form of modal parameters such as the natural frequency, mode shape, and modal damping ratio. The modal parameters indicate the unique properties of a structure, and during structure damage, the values of structure mass, stiffness, or damping and consequently their corresponding modal parameters change. consequently, damage identification in the structure could be performed by analysis of the modal parameters [28–32]. In some research works, the wavelet transform of modal parameters is used for detecting damages in structures [33–35].

In recent years the contourlet transform (CT) which is a multi-scale directional transform is introduced as an alternative to the wavelet transform for detecting damages with complex geometric shapes in 2D structures [36]. For instance, Shahrokhinasab et al. [37] investigate the performance of image-based crack detection systems in concrete structures. Ma et al. [38] have utilized the contourlet transform for identifying road pavement distress. The capability of contourlet transform for crack identification in roads has been also examined in some other research works [39–41]. Ai and Xu [42] used the contourlet transform for damage detection in metal plates. In the research of Hajizadeh et al. [43] the performances of wavelet transform and contourlet transform concerning the damage identification in plate-like structures were compared to each other. The results showed that the contourlet transform in addition to damage localization is capable of detecting the geometric shape of damages. Li et al. [44] could accurately identify the surface defects by taking images before and after damages at the surfaces made of nickel alloy and processing the images using the contourlet transform. They concluded that the proposed method could detect surface defects with 88.9% precision. Vafaei and Salajegheh [45] used the wavelet transform and contourlet transform for detecting curved shaped damages in the plate structures with fixed supports. The results of investigations showed that the contourlet transform could better detect the curved-shaped damages with respect to the wavelet transform.

2. Research significance

The previous research works show that the wavelet transform is capable of identifying various damage types in one-dimensional structures and single damages in two-dimensional structures. But as the 2D wavelet transform is the extended form of the 1D wavelet transform, application of wavelet transform on 2D structures especially for inclined and curved damages does not yield desirable results. Instead, contourlet transform (CT) is introduced as an alternative to the wavelet transform for detecting damages with complex geometric shapes in 2D structures. Up to now, little research works have been conducted on damage identification in structures using the contourlet transform method. In this paper, the contourlet transform has been used for damage detection in the prestressed concrete slabs, as one of the most common structural elements in recent years. For this purpose, the numerical models of the prestressed concrete slab were built based on the experimental specimens reported in the previous research works. Next, the single, double, and triple damage scenarios with different geometric shapes (transverse, longitudinal, inclined, and curved slots) and at different locations (middle and corners) were created in them. In the modeling, the depth of slots in the single and double damages is taken constant and for the triple ones is taken variable, to assess the severity of damages. For detecting the damage scenarios, the first mode shape of each numerical model for the two damaged and undamaged states is obtained. Then, to improve the sensitivity of the damage identification method, the curvature of the mode shapes has been used rather than the vibration mode shapes. The contourlet transform coefficients corresponding to curvature modals of the first mode shape of the prestressed concrete slab per each damage scenario, and for two states of the damaged and undamaged structure are taken as the inputs for the proposed damage index. The maximum values of the proposed damage index are selected to represent the severity of that damage and the corresponding locations, where these maximum values occur, are selected as the locations of the estimated damages. The proposed damage index could be beneficial for engineers and researchers who are active in damage detection and structural health monitoring field.

3. Method

3.1. Contourlet transform

Signal processing methods are known as one of the efficient methods for damage identification in the structures. The basis of most of these methods is the Fourier transform. In the Fourier transform, the signal is transformed from the time domain to the frequency domain. During this transformation, a portion of the signal time information is lost. Regarding this deficiency, the wavelet transform was introduced as an appropriate alternative to the Fourier transform. The wavelet transform is a method for signal processing that provides the possibility of time windowing with variable dimensions. This transform by focusing on the short time interval for high-frequency components and focusing on the long time interval for low-frequency components improves analysis of the signals with fluctuations and local changes [46]. The performance of wavelets is very good in one-dimensional signals. Nevertheless, in most cases, the extended form of one-dimensional wavelets used for processing the 2D signals. Hence, the wavelet transforms have not an appropriate performance in processing signals with higher

dimensions and there is a need for other signal processing methods with higher capabilities. The contourlet transform is a new generation of signal processing methods that has fixed the deficiencies of the wavelet method for the analysis of multi-dimensional signals.

The contourlet transform is a transform with a directional multi-scale structure which utilizes the double filter banks in sequences. In this structure, first, the Laplacian Pyramid (LP) detects the point discontinuities over the input signal [47]. Then, to attach the point discontinuities and linear structures, the directional filter bank (DFB) is used [48]. Fig. 1 shows an example of the contourlet transform. The bandpass signal obtained from LP is passed through DFB to perform decomposition in its different directions. This operation could be continued on the lowpass signal [49]. The result of this decomposition is a kind of signal representation where it is comprised of the original signals as the contour sections in various directions and scales and for this reason, is called contourlet.

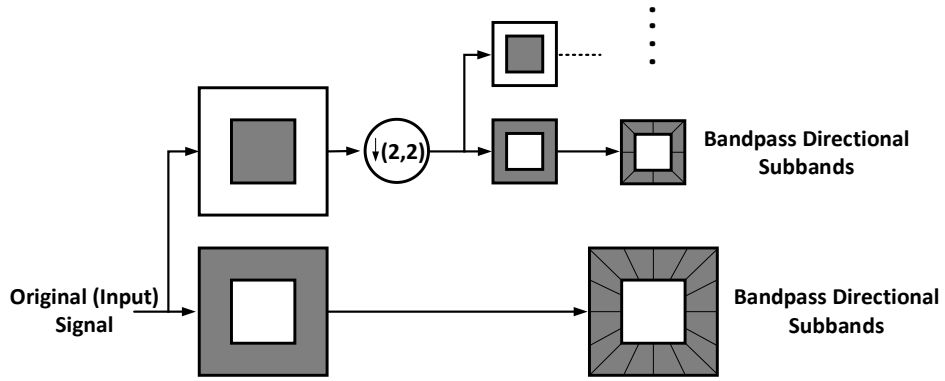

Fig. 1. Multiscale decomposition using the Laplacian Pyramid (LP) and applying the Directional Filter Bank on each bandpass signal in the contourlet transform [49].

Per each input signal, *x*, the LP decomposition at each stage creates a downsampled lowpass signal (coarse signal)(*c*) from the original signal and a bandpass signal (detail signal)(*d*), in the form of difference between the original signal, *x*, and its corresponding estimated value, *p*. The LP decomposition is shown in Fig. 2 where *H* and *G* denote the one-dimensional lowpass analysis and synthetic filter, respectively and M represents the sampling matrix. After Laplacian decomposition, the bandpass signal, *d*, is decomposed using the directional filter bank [50].

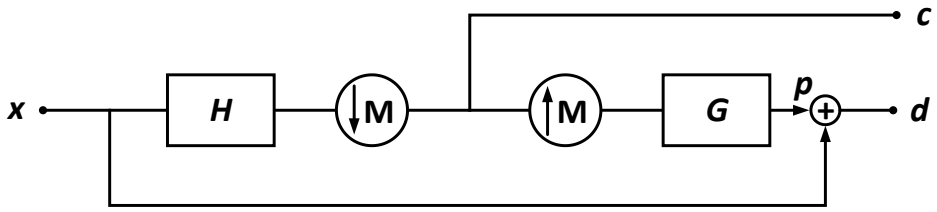

Fig. 2. Coarse approximation, *c*, and difference, *d*, between the original signal and the estimated value *p*, by Laplacian Pyramid (LP) decomposition [50].

In the certain regularity condition, the lowpass synthesis filter, *G*, defines a unique scaling function, $\varphi(t) \in L_2(R^2)$ that satisfies the following two-scale equation [50]:

$$\varphi(t) = 2 \sum_{n \in Z^2} g[n] \varphi(2t - n) \tag{1}$$

Considering $\varphi_{j,n} = 2^{-j}\varphi\left(\frac{t-2^j n}{2^j}\right)$, $j \in Z$, $n \in Z^2$, then the family $\{\varphi_{j,n}\}_{n\in Z^2}$ is orthonormal which consists of an approximation subspace V_j at the scale 2^j. $\{V_j\}_{j\in Z}$ is a sequence of multiresolution nested subspaces $..V_2 \subset V_1 \subset V_0 \subset V_{-1} \subset V_{-2}...$ in which V_j is related to a uniform grid of $2^j \infty\ 2^j$ intervals that characterizes the signal approximation at scale 2^j [50].

The detail (difference) signals, *d*, exist within the subspace W_j which is the orthogonal component of V_j in V_{j-1} or $V_{j-1} = V_j \oplus W_j$. Now, LP could be considered as an oversampled filter bank where each polyphase component of detail (difference) signal, *d*, together with the coarse signal, *c*, comes from a separate filter bank channel. By assuming $F_i(z),\ 0 \le i \le 3$ as the synthesis filters for the multiple phase components, which are the highpass filters, each of these filters could be related with a continuous function $\psi^{(i)}(t)$ as shown in Eq. (2) [50]:

$$\psi^{(i)}(t) = 2\sum_{n\in Z^2} f_i[n]\varphi(2t-n) \tag{2}$$

Assuming $\psi^{(i)}{}_{j,n}(t) = 2^{-j}\psi^{(i)}\left(\frac{t-2^j n}{2^j}\right)$, $j \in Z$, $n \in Z^2$ in scale 2^j, $\{\psi^{(i)}_{j,n}\}_{0\le i\le 3,\ n\in Z^2}$ is a tight frame for W_j. For all scales, $\{\psi^{(i)}_{j,n}\}_{j\in Z,\ 0\le i\le 3,\ n\in Z^2}$ is a tight frame for $L_2(R^2)$ and in both cases, the frame bounds are equal to 1 [50].

As the multiscale and directional decomposition are separated in the discrete contourlet transform, a different number of directions with different scales are created which resulting in a flexible multiscale and directional expansion. Furthermore, the full binary tree decomposition of the DFB in the contourlet transform could be generalized to arbitrary tree structures. The result is a family of directional multiresolution expansions, which similar to the wavelet packets, are called contourlet packets. Fig. 3 shows an example of possible frequency decompositions by the contourlet transform and contourlet packets [39]:

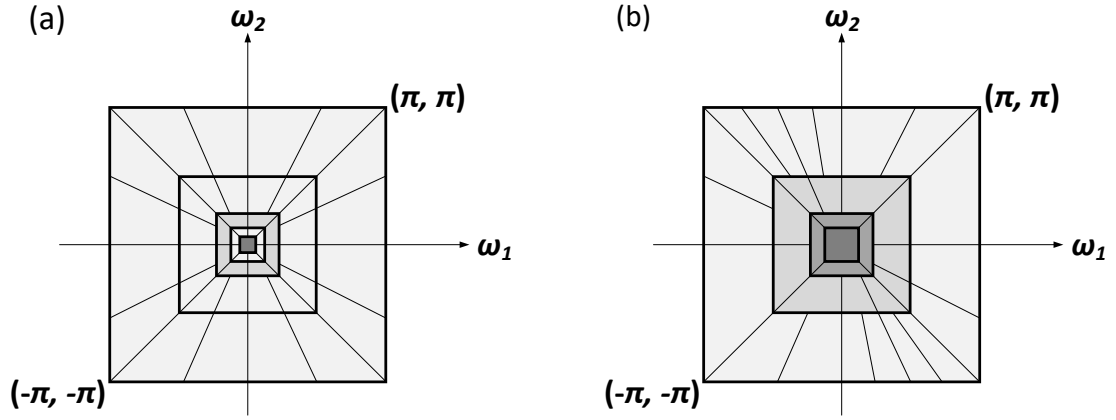

Fig. 3. An example of possible frequency decompositions using: a) contourlet transform; b) contourlet packets [39].

Fig. 3 shows that the contourlet packets provide finer angular resolution decomposition at any scale or direction with respect to the contourlet transform. Hence, the flexibility of contourlet packets causes that this transform could better smooth contours of various curvatures [39].

Assuming $x = a_0[n]$ as the input signal, the output of LP stage is J bandpass signals $b_j[n]$, j = 1,2,….,J (in the fine to coarse order) and a lowpass signal $a_J[n]$. This means that the jth level, the LP decomposes the signal $a_{j-1}[n]$ into a coarser signal $a_j[n]$ and detail signal $b_j[n]$. Then, each bandpass signal $b_j[n]$ is further decomposed by an l_j -level DBF into 2^{l_j} bandpass directional signals $c_{j,k}^{(l_j)}[n]$, $k = 0,1,...,2^{l_j-1}$ [50]. If $a_0[n] = \langle f, \varphi_{L,n} \rangle$ is inner products of a function $f(t) \in L_2(R^2)$ with the scaling function at scale L and the signal $a_0[n]$ is decomposed by the discrete contourlet transform into coefficients $\left\{a_J[n], c_{j,k}^{(l_j)}[n]\right\}$, $j = 1,2,...,J$, $0 \le k < 2^{l_j} - 1$, then the coefficients $a_J[n]$ and $c_{j,k}^{(l_j)}[n]$ could be calculated by Eq. (3) and Eq. (4), respectively [50]:

$$a_J[n] = \langle f, \varphi_{L+J,n} \rangle \tag{3}$$

$$c_{j,k}^{(l_j)}[n] = \langle f, \lambda_{L+j,k,n}^{(l_j)} \rangle \tag{4}$$

In which, $\lambda_{j,k,n}^{(i)}(t)$ could be obtained from Eq. (5):

$$\lambda_{j,k,n}^{(i)}(t) = \sum_{m \in Z^2} d_k^{(l)} \left[m - S_k^{(l)} n \right] \mu_{j,m}(t), \mu_{j,2n+k_i}(t) = \psi_{j,n}^{(i)}(t), \ 0 \le i \le 3 \tag{5}$$

In Eq. (5), the overall sampling matrices $S_k^{(l)}$ in the contourlet transform have the diagonal forms as shown in Eq. (6):

$$S_k^{(l)} = \begin{cases} diag(2^{l-1}, 2) & 0 \le k \le 2^{l-1} \\ diag(2, 2^{l-1}) & 2^{l-1} \le k \le 2^l \end{cases} \tag{6}$$

In this paper, by considering the modal curvatures, corresponding to the first mode of the prestressed concrete slab models in two damaged and undamaged states, as inputs of the contourlet transform, the detail coefficients $c_{j,k}^{(l_j)}[n]$ are utilized for damage identification.

3.2. Numerical models and validation

In this paper, one of the prestressed concrete slab specimens tested in the Pahlevan Mosavari [51] research work has been used for building the numerical models. They used modal testing to obtain the modal data of some prestressed concrete slab specimens with dimensions of 60cm×160cm and thicknesses of 10, 15, and 20cm. Concrete material with compressive strength of 30MPa and steel cables with 4.97mm diameter and cover of 25mm were used to manufacture the experimental specimens of that research. Table 1 and Fig. 4 show the mechanical properties of the materials and cross-sectional view of the selected experimental prestressed concrete slabs, respectively.

Table 1
Mechanical properties of the concrete and steel materials [51].

Materials	Density (kg/m^3)	Elastic modulus (GPa)	Poisson's ratio
Concrete	2200	23.5	0.2
Steel	8750	200	0.3

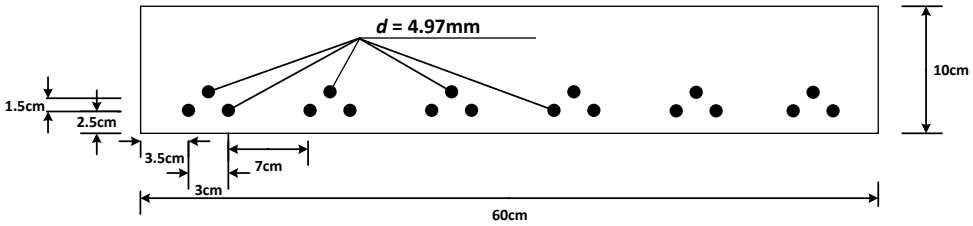

Fig. 4. Cross-section of the selected prestressed concrete slab [51].

In the Pahlevan Mosavari [51] research work, to achieve the modal parameters, modal testing conducted using an impact hammer and an accelerometer. For that purpose, as shown in Fig. 5, each specimen was hanged by two elastic bands to reduce the effects of boundary conditions. Degrees of freedoms were considered as a set of nodes with 10cm intervals on the upper surface of each specimen. The natural frequencies and mode shapes of each specimen were obtained using the frequency response functions (FRFs) by measuring the impact force, which was applied at each degree of freedom, and the responses received from the accelerometer, which was installed at the middle of the slab.

Fig. 5. Conducting modal testing on prestressed concrete slab specimen in a hanged position [51].

In this paper, one of the prestressed concrete slab specimens of Pahlevan Mosavari research work [51] with 10cm thickness is selected and modeled in ABAQUS software. To model concrete materials, the plastic damage model in the ABAQUS software library has been used which was first proposed by Lubliner et al. [52]. In this model, the two modes of cracking and softening are assumed in the tension and compression behavior of concrete materials, respectively. Consequently, when the concrete material cracks in tension or crushes in compression, a definite

value of the damage is considered at every point of the stress-strain curve. These tensile and compressive damage values were calculated utilizing the assumption of Onate et al. [53], in which, the amount of damages is considered zero, before the stresses in the material reach tensile and compressive strength values. By increasing the tensile cracking or compressive crushing in concrete material, the tensile and compressive damage value increases. In order to model the prestressed bars, a comprehended contact between them and surrounding concrete is assumed and a truss-like behavior is considered for them. According to the properties presented in Table 1, a bilinear stress-strain behavior is assumed for steel material. nonlinear analyses including the contact, large deformations, plasticity, and damage analysis [54] were applicable in this paper by selecting the C3D20 element with 20 nodes, where each node has three components of translation degrees of freedom, and truss element T3D3 for meshing of the concrete and steel materials, respectively. Different sizes of meshing were selected and the most optimal one was adopted to achieve a suitable meshing with natural frequencies close to the experimental results. As shown in Fig. 6, the most proper dimensions of optimal meshes were obtained equal to cubics with 20mm sides. The sensor location with coordinate (100, 30) in XY plate is also indicated.

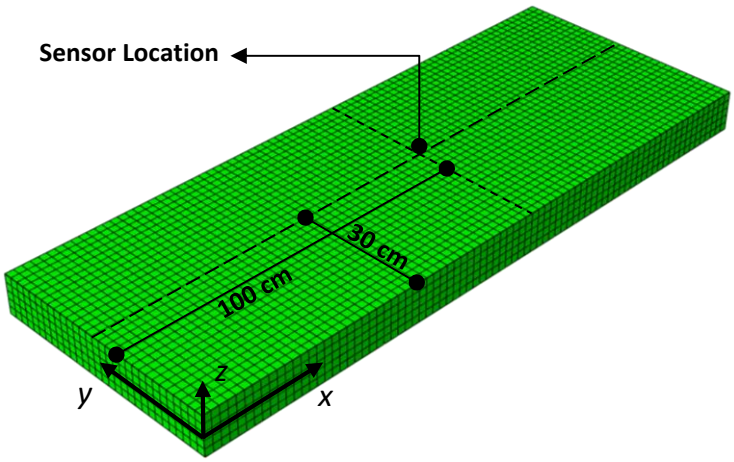

Fig. 6. Numerical model meshing.

Prestressing action is simulated by defining initial stresses in steel cables. Initial stresses of 7156 kg/cm^2 and 9600 kg/cm^2 are considered for the upper and lower rebars (Fig. 4), respectively. A negative deflection is induced in numerical models of prestressed concrete slabs by applying the initial. The first three mode shapes of the prestressed concrete slab model are illustrated in Fig. 7 and their corresponding natural frequencies are compared with the results obtained from modal testing in the Pahlevan Mosavari research [51] in Table 2.

Table 2
Natural frequencies comparison between the experimental specimen and numerical model

Mode Number	Natural frequencies (Hz)		Erorr Value (%)
	Experimental Specimen [51]	Numerical Model	
First	125.1	128.4	2.64
Second	201.8	207.9	3.02
Third	341.2	346.2	1.47

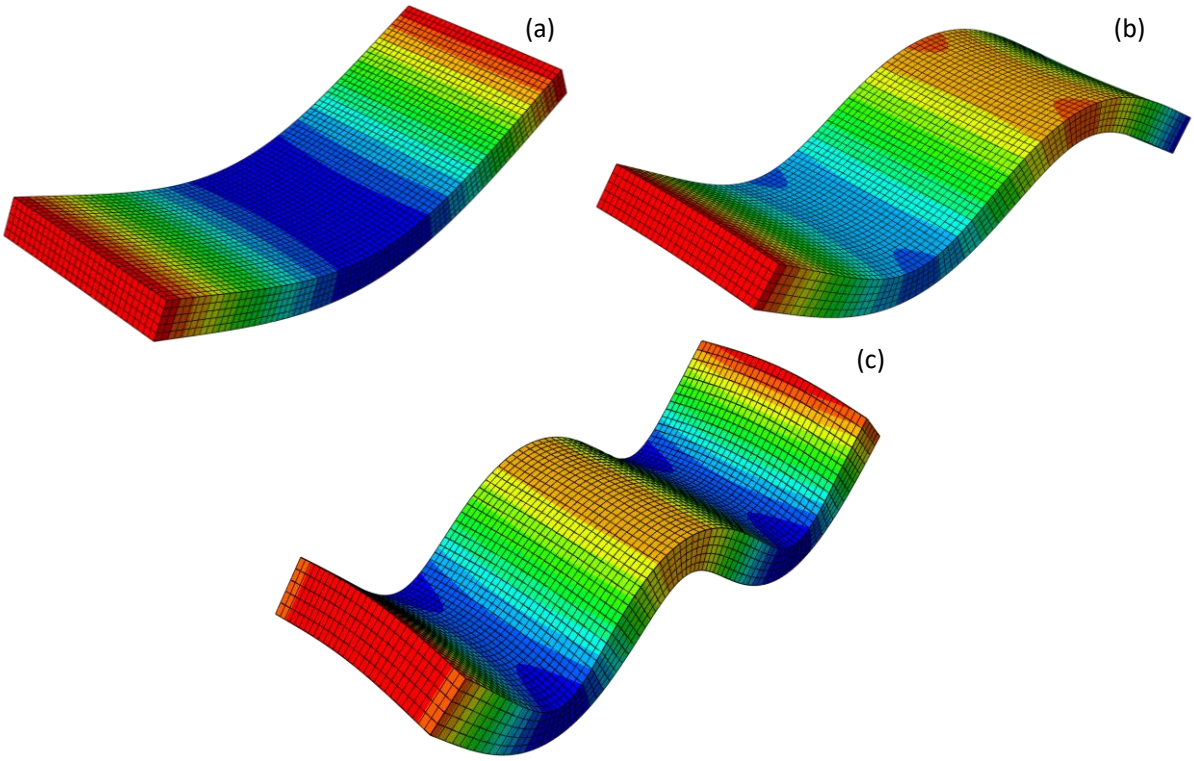

Fig. 7. Mode shape of the prestressed concrete slab model: a) first mode; b) second mode and c) third mode.

Table 2 shows that, although some negligible differences exist between the frequencies in the numerical model and those in the experimental specimens due to the inability in providing full hanging condition in the experimental conditions, the obtained natural frequencies of the numerical model in this paper are in well consistent with those resulted by the modal testing on the prestressed concrete slab specimens in the Pahlevan Mosavari research [51] and the numerical model confidentially could be used.

3.3. Damage scenarios

In this paper, three damage scenarios, namely the single, double and triple, with different geometric shapes and at different locations were created in the numerical models of prestressed concrete slabs. The precise location of each damage scenario, in terms of the defined coordinate system, is illustrated in Fig. 8.

According to Fig. 9, in this paper, four types of geometric shapes were used to create damage scenarios in numerical models. These damages are assumed as transverse slots (TS), longitudinal slots (LS), inclined slots (IS) with 10mm width and 60mm length, and curved slots (CS) with 10mm width and 60mm outer diameter. In the single and double damage scenarios, the depth of these slots is taken constant and equal to 20mm. In the triple damage scenarios, to assess the severity of damages, the depth is assumed variable with 5, 10,20,30,40, and 50mm dimensions.

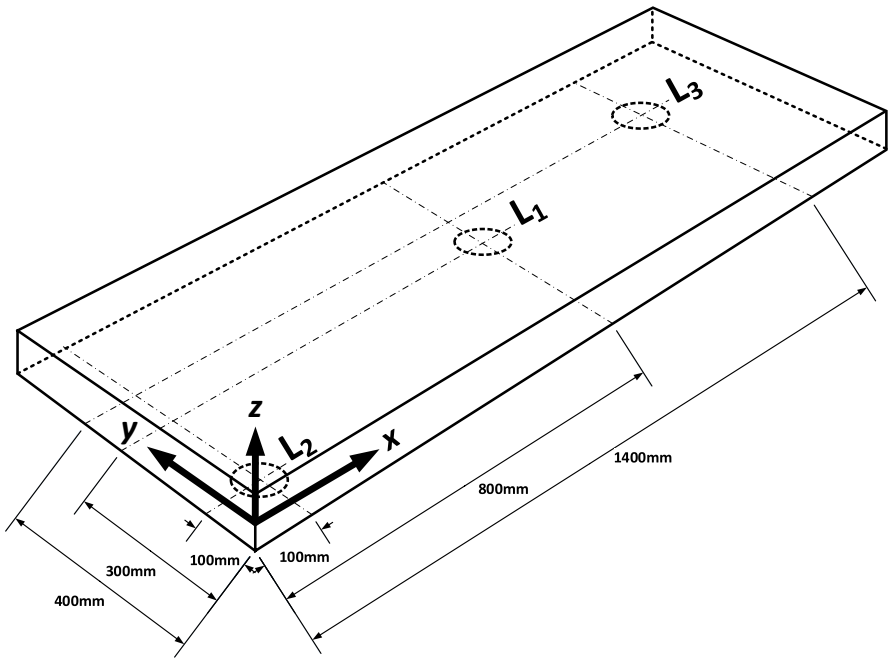

Fig. 8. Locations of different damage scenarios: L_1, L_2 and L_3.

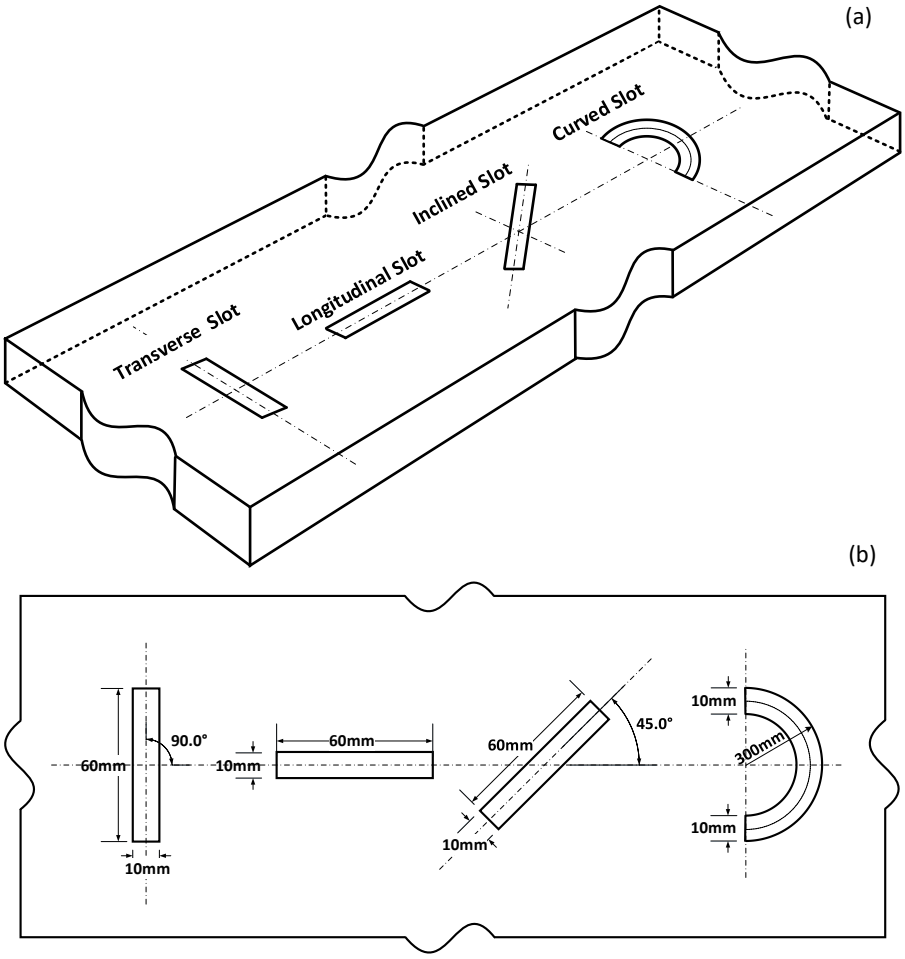

Fig. 9. Geometric shapes of the damage scenarios: a) 3D view; b) Plan view

3.4. Proposed damage index

In this paper, to detect the location and severity of each damage scenario, the first mode shape of the prestressed concrete slab numerical models in two damaged and undamaged states was obtained. Then, to increase the sensitivity of the damage identification method, the curvature mode shapes were used instead of the mode shapes. Pandey et al. [55] were the first researchers who suggested that the use of the curvature mode shape, or the second derivative of mode shape, yields a higher sensitivity to the damage and could be incorporated for damage localization. The curvature of mode shapes at *i*th element node could be derived using the central difference approximation as shown below:

$$w_i'' = \frac{\left(w_{i+1} - 2w_i + w_{i-1}\right)}{h^2} \tag{7}$$

In Eq. (7), h is the distance between the (i-1) and (i+1)th element nodes and the ith element node in the structure and w_i is the mode shape value at the ith element node. By a generalization of Eq. (7), the curvature mode shape for 2D structures at (i,j) element node could be obtained by implementing the central difference approximation according to Eq. (8) [56]:

$$w_{i,j}'' = \frac{\left(w_{i+1,j+1} - w_{i+1,j} - w_{i,j+1} + 2w_{i,j} - w_{i-1,j} - w_{i,j-1} + w_{i-1,j-1}\right)}{2h_i h_j} \tag{8}$$

In Eq. (8), h_i and h_j are the longitudinal and transverse distances between the (i-1)th and (j-1)th and (i+1)th and (j+1)th element nodes and the (i,j)th element node, respectively. $W_{i,j}$ is the mode shape value at (i,j)th element node. The curvature mode shapes corresponding to the first mode shape of prestressed concrete slab models in two damaged and undamaged states are taken as inputs for the proposed damage index $DI_{i,j}$:

$$DI_{i,j} = \frac{C_{d_{i,j}} - C_{u_{i,j}}}{\max(C_{u_{i,j}})} \tag{9}$$

In Eq. (9), The damage index $DI_{i,j}$ is the result of subtracting the coefficients obtained by applying the contourlet transform on curvature mode shapes of the first vibration mode shape of damaged, $C_{d_{i,j}}$, and undamaged, $C_{u_{i,j}}$, numerical models with respect to the maximum coefficient value in the undamaged state. The maximum values of the proposed damage index $DI_{i,j}$ represent the damage severity and, the location of these maximum values represents the location of estimated damages.

4. Results

4.1. Single damage scenarios

In this paper, 12 single damage scenarios with different geometric shapes and at different locations of the prestressed concrete slab models were created, where the notation of S_L_i,T_a is used for their designation. In this notation, S denotes the single damage scenario, L_i denotes the

location of damage (L_1, L_2, and L_3) and T_a denotes the damage type (TS, LS, IS, and CS for transverse, longitudinal, inclined, and curved slots, respectively). Based on the damage locations, the numerical models of the prestressed concrete slabs containing single damage scenarios were classified into three groups of S_L_1, S_L_2, and S_L_3. The geometric properties and the maximum value obtained from the damage index $DI_{i,j}$ per each single damage scenario are given in Table 3.

Table 3
Geometric properties and maximum value of damage index $DI_{i,j}$ for single damage scenarios.

Damage Scenario		Damage Location	Damage Type	Damage Index $DI_{i,j}$
Group	**Name**			
S_L_1	S_L_1,TS	L_1	Transverse Slot	0.3396
	S_L_1,LS		Longitudinal Slot	0.0332
	S_L_1,IS		Inclined Slot	0.2488
	S_L_1,CS		Curved Slot	0.4791
S_L_2	S_L_2,TS	L_2	Transverse Slot	0.0273
	S_L_2,LS		Longitudinal Slot	0.0035
	S_L_2,IS		Inclined Slot	1.6887
	S_L_2,CS		Curved Slot	1.6070
S_L_3	S_L_3,TS	L_3	Transverse Slot	0.0773
	S_L_3,LS		Longitudinal Slot	0.0050
	S_L_3,IS		Inclined Slot	1.7137
	S_L_3,CS		Curved Slot	0.7205

The results of the proposed damage index $DI_{i,j}$ for prestressed concrete slab models with single damage scenarios of S_L_1, S_L_2, and S_L_3 groups are given in Figs. 10, 11, and 12, respectively.

The results of Table 4 and Fig. 10 show that the proposed damage index $DI_{i,j}$, has a good capability in identifying each of the single damage scenarios with geometric shapes of TS, LS, IS, and CS at location L_1. The maximum value of the damage index in the group S_L_1 belongs to damages with the geometric shape of CS. Moreover, the damage scenarios with geometric shapes of TS, IS and LS have the highest value of damage index $DI_{i,j}$, respectively.

Fig. 11 shows that applying the proposed damage index $DI_{i,j}$ on the prestressed concrete slab models in S_L_2 group has resulted in well identification of single damage scenarios with geometric shapes of TS, LS, IS, and CS at location L_2. Investigation of the maximum values of the damage index in the S_L_2 group given in Table 4, shows higher sensitivity of this index to IS geometric shape. After that, the single damage scenarios with geometric shapes of CS, TS, and LS have the highest value of damage index $DI_{i,j}$, respectively.

Similar to S_L_1 and S_L_2 groups, the results of Fig. 12 shows that the proposed damage index DIi,j also has the capability of detecting single damage scenarios in S_L_3 group with geometric shapes of TS, LS, IS, and CS. As the same results obtained from S_L_2 group, in S_L_3 group also the damage index has shown the highest sensitivity to damage scenarios with IS geometric shape and then are ranked the geometric shapes CS, TS, and LS, respectively.

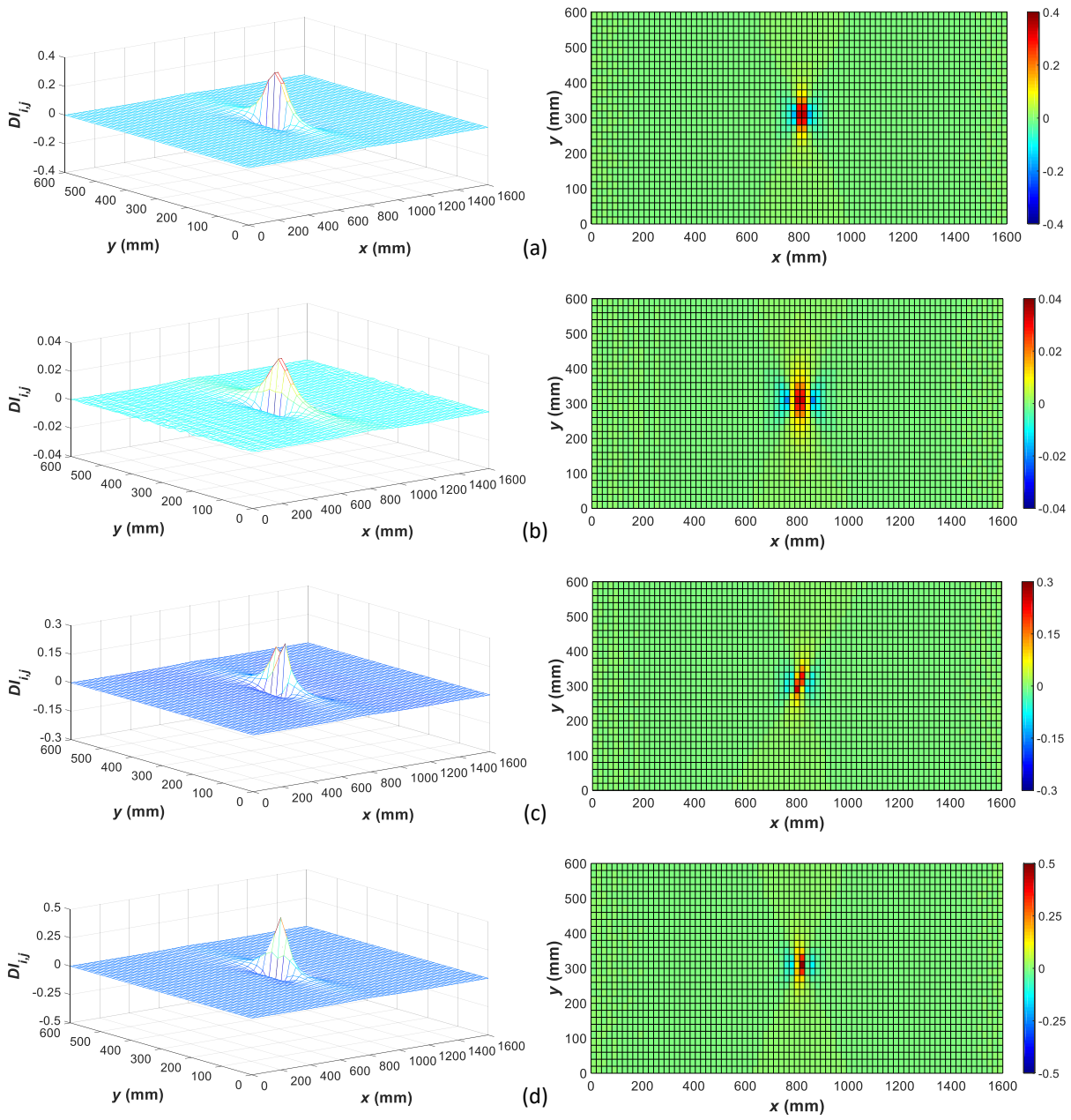

Fig. 10. Single damage scenarios identification of S_L$_1$ group using the damage index $DI_{i,j}$: a) S_L$_1$,TS; b) S_L$_1$,LS; c) S_L$_1$,IS and d) S_L$_1$,CS.

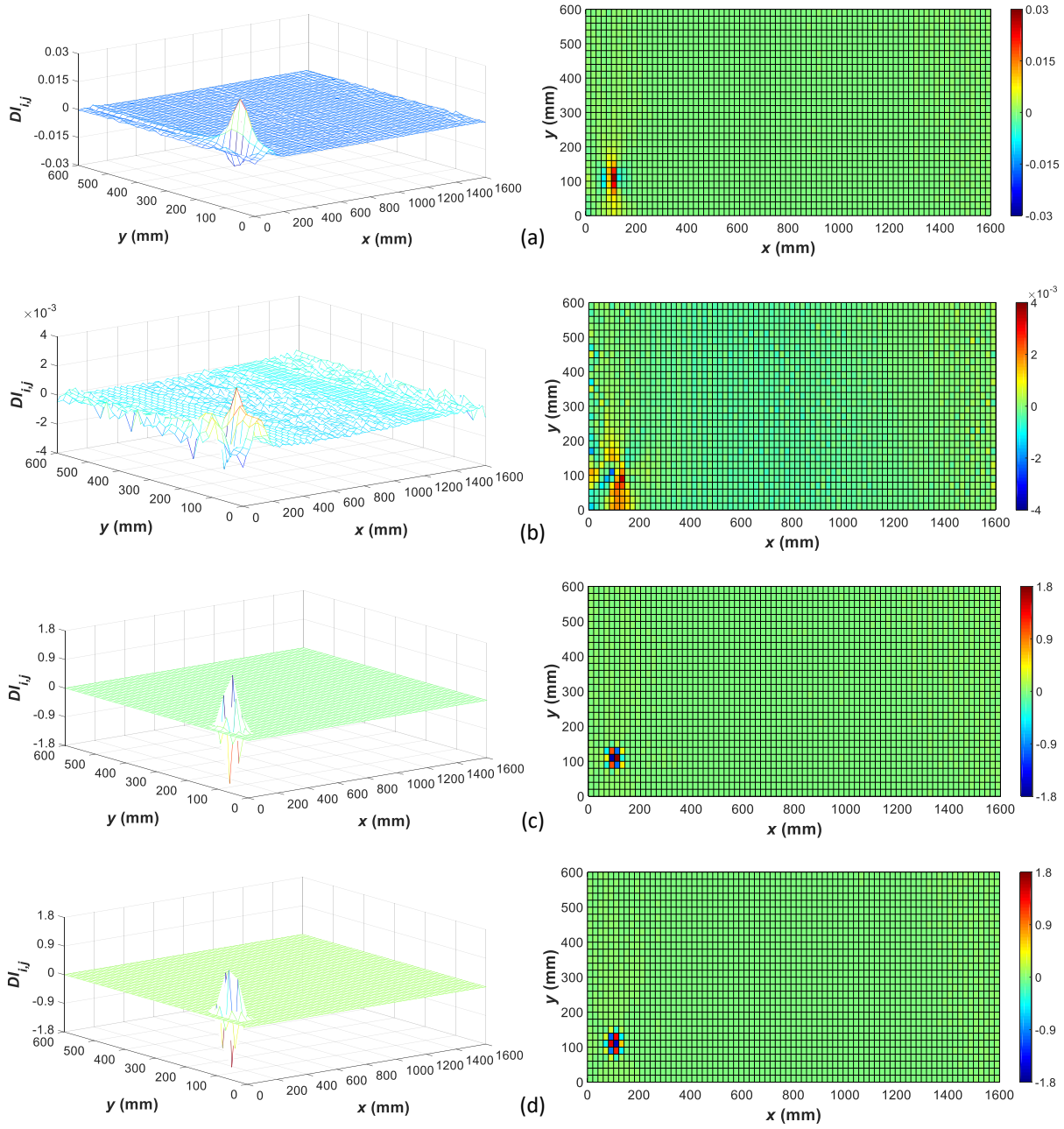

Fig. 11. Single damage scenarios identification of S_L$_2$ group using the damage index $DI_{i,j}$: a) S_L$_2$,TS; b) S_L$_2$,LS; c) S_L$_2$,IS and d) S_L$_2$,CS.

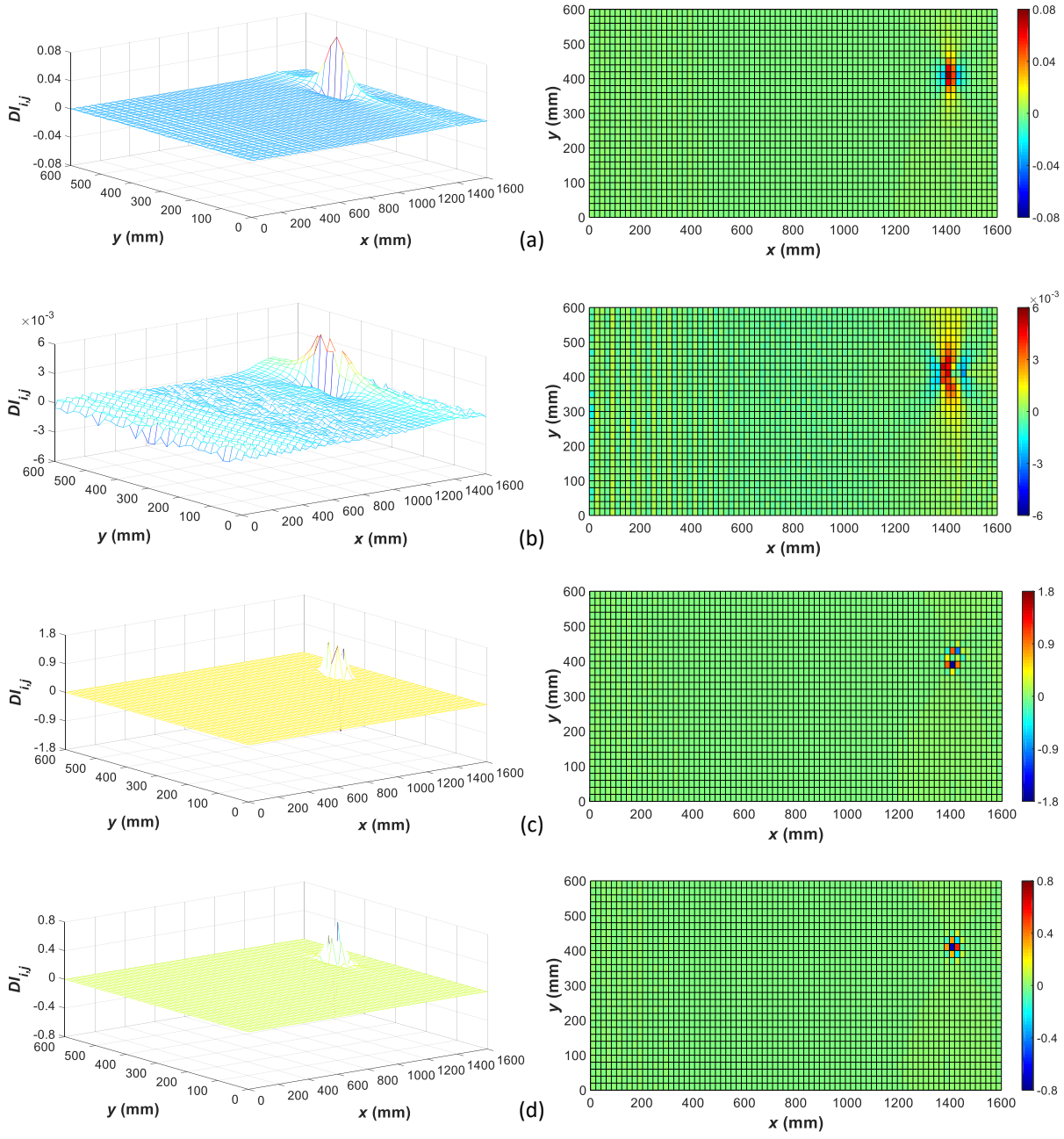

Fig. 12. Single damage scenarios identification of S_L_3 group using the damage index $DI_{i,j}$: a) S_L_3,TS; b) S_L_3,LS; c) S_L_3,IS and d) S_L_3,CS.

4.2. Double damage scenarios

In order to investigate the capability of the proposed damage index $DI_{i,j}$, in addition to the single damage scenarios, 8 combinations of double damage scenarios with different geometric shapes and at different locations of the prestressed concrete slab models were created. The double damage scenarios were labeled by D_L_i,T_a_L_j,T_b notation in which, D represents the double damage scenario, L_i and L_j denote the location of damages (L_1, L_2, and L_3), and T_a and T_b

illustrate the damage type (TS, LS, IS and CS). Based on the location of damages, the numerical models of the prestressed concrete slabs with double damage scenarios were classified into 3 groups of D_L_1_L_2, D_L_1_L_3 and D_L_2_L_3. Table 4 demonstrates the geometric properties and maximum values of damage index $DI_{i,j}$ per each double damage scenario in the prestressed concrete slab models.

Table 4
Geometric properties and maximum value of damage index $DI_{i,j}$ for double damage scenarios.

Damage Scenario			**Damage Location**	**Damage Shape**	**Damage Index $DI_{i,j}$**
Group	**Name**				
D_L_1_L_2	D_L_1,TS_L_2,TS	L_1,TS	L_1	Transverse Slot	0.3401
		L_2,TS	L_2	Transverse Slot	0.0271
	D_L_1,CS_L_2,CS	L_1,CS	L_1	Curved Slot	0.4784
		L_2,CS	L_2	Curved Slot	0.7741
	D_L_1,LS_L_2,IS	L_1,LS	L_1	Longitudinal Slot	0.0329
		L_2,IS	L_2	Inclined Slot	1.0970
D_L_1_L_3	D_L_1,LS_L_3,LS	L_1,LS	L_1	Longitudinal Slot	0.0331
		L_3,LS	L_3	Longitudinal Slot	0.0049
	D_L_1,TS_L_3,IS	L_1,TS	L_1	Transverse Slot	0.3402
		L_3,IS	L_3	Inclined Slot	1.0827
	D_L_1,CS_L_3,LS	L_1,CS	L_1	Curved Slot	0.4788
		L_3,LS	L_3	Longitudinal Slot	0.0043
D_L_2_L_3	D_L_2,IS_L_3,IS	L_2,IS	L_2	Inclined Slot	1.6579
		L_3,IS	L_3	Inclined Slot	1.6564
	D_L_2,CS_L_3,TS	L_2,CS	L_2	Curved Slot	0.7743
		L_3,TS	L_3	Transverse Slot	0.0771

Figs. 13, 14 and 15 show the results of proposed damage index $DI_{i,j}$ in the prestressed concrete slab models with double damage scenarios in groups D_L_1_L_2, D_L_1_L_3, and D_L_2_L_3, respectively.

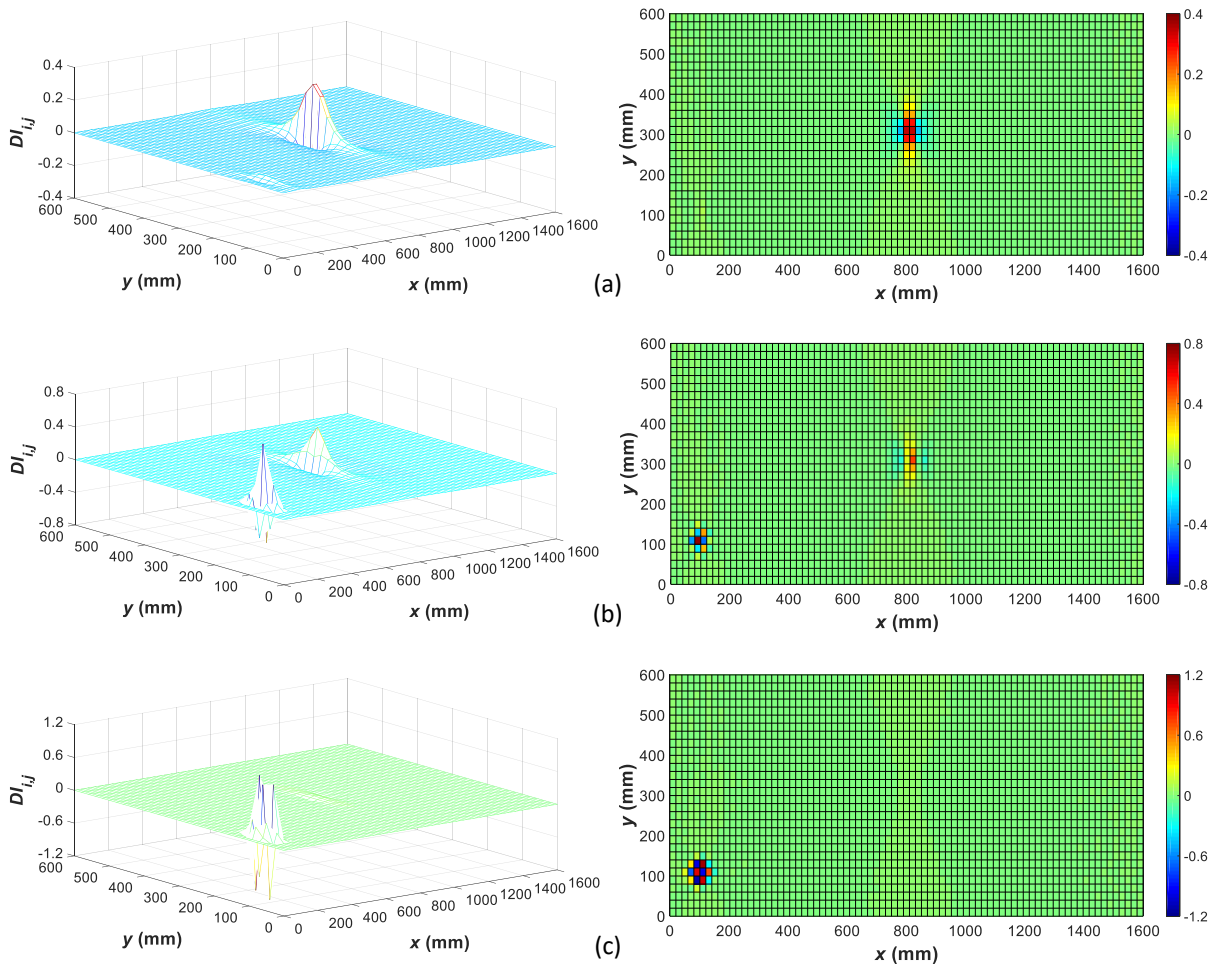

Fig. 13. Double damage scenarios identification of D_L_1_L_2 group using the damage index $DI_{i,j}$: a) D_L_1,TS_L_2,TS; b) D_L_1,CS_L_2,CS and c) D_L_1,LS_L_2,IS.

Investigating the results of Table 4 and Fig. 13 shows that the proposed damage index $DI_{i,j}$, has a well capability in identifying each double damage scenario with geometric shapes of TS, LS, IS and CS at locations L_1 and L_2. But there is a difference in the damage index sensitivity to some damages and locations with respect to others. Fig. 13(a) shows that in the D_L_1,TS_L_2,TS model, which has similar damage scenarios of TS at locations L_1 and L_2, the proposed damage index has a higher sensitivity to location L_1 with respect to L_2. On the contrary, according to Fig. 13(b), the proposed damage index for the D_L_1,CS_L_2,CS model, which has similar damage scenarios of CS at locations L_1 and L_2, has approximately an equal sensitivity to locations L_1 and L_2. On the other hand, the obtained results of Fig. 13(c) shows that in D_L_1,LS_L_2,IS model, which has damages LS and IS at locations L_1 and L_2, respectively, the damage index has a higher sensitivity to damage IS at location L_2 with respect to damage LS at location L_1.

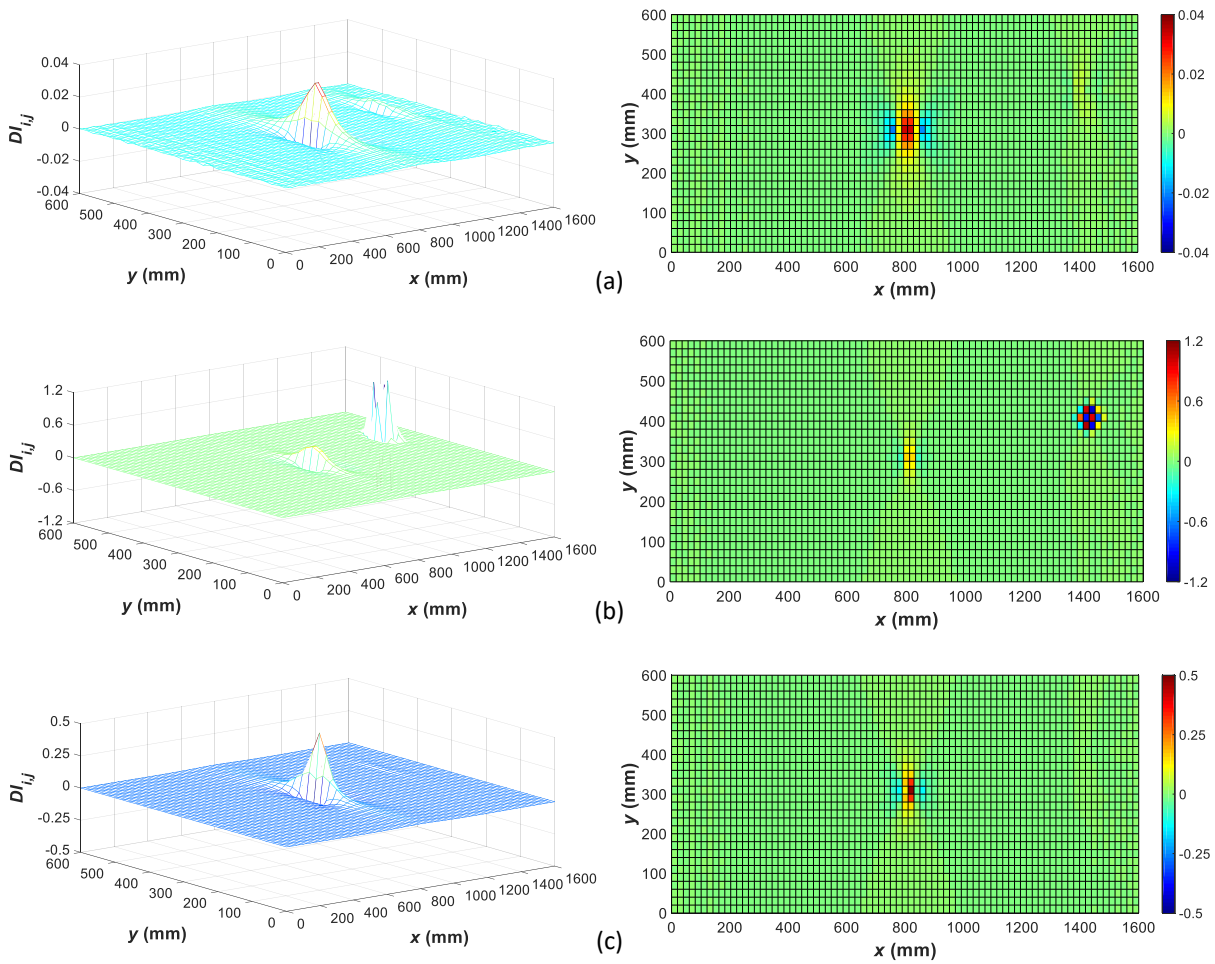

Fig. 14. Double damage scenarios identification of D_L_1_L_3 group using the damage index $DI_{i,j}$: a) D_L_1,LS_L_3,LS; b) D_L_1,TS_L_3,IS and c) D_L_1,CS_L_3,LS.

The results obtained for D_L_1,LS_L_3,LS model, with similar damage scenarios of LS type at locations L_1 and L_3, as shown in Fig. 14(a), shows that for damage type LS, the damage index sensitivity to the damage location L_1 is higher than location L_3. Fig. 14(b) shows that in D_L_1,TS_L_3,IS model, which has damage scenarios of TS and IS at locations L_1 and L_3, respectively, the damage index has a higher sensitivity to damage IS at location L_3 with respect to damage TS at location L_1. Furthermore, according to Fig. 14(c), the proposed damage index for D_L_1,CS_L_3,LS model, containing damage scenarios of CS and LS at locations L_1 and L_3, respectively, has a higher sensitivity to the damage CS at location L_1 with respect to damage LS at location L_3.

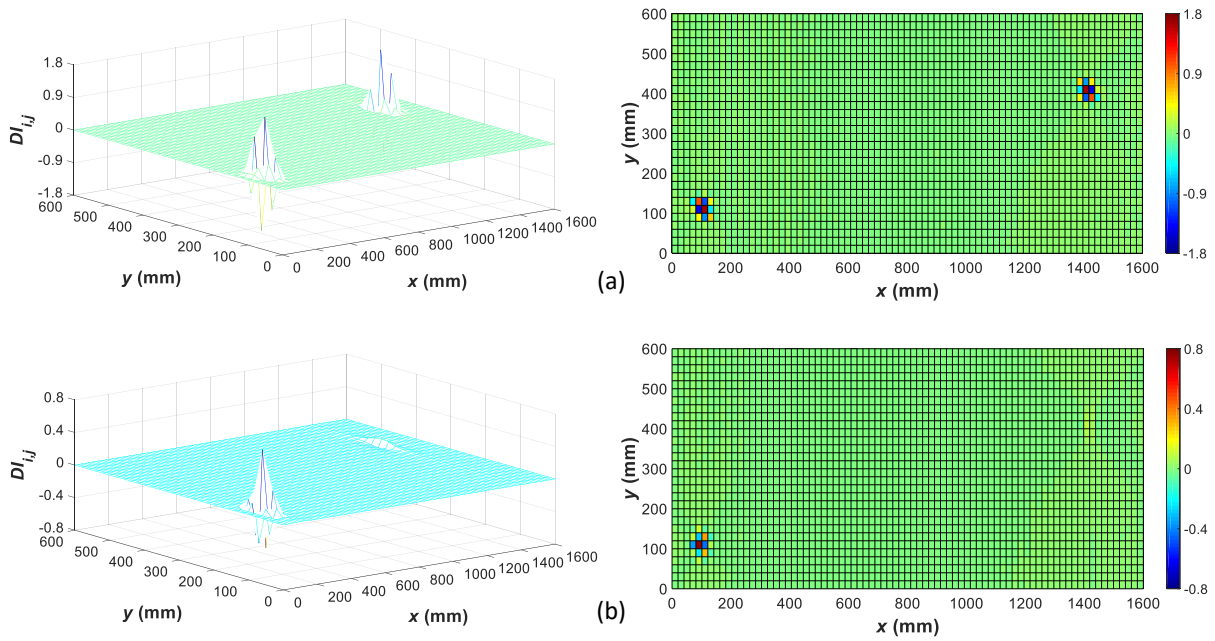

Fig. 15. Double damage scenarios identification of D_L_2_L_3 group using the damage index $DI_{i,j}$: a) D_L_2,IS_L_3,IS and b) D_L_2,CS_L_3,TS.

Fig. 15(a) shows that in D_L_2,IS_L_3,IS model, which has similar damage scenarios of IS at locations L_2 and L_3, the proposed damage index has equal sensitivity to locations L_2 and L_3. On the other hand, according to Fig. 15(b), the proposed damage index for D_L_2,CS_L_3,TS model, with damage scenarios of CS and TS at locations L_2 and L_3, respectively, has a higher sensitivity to damage CS at location L_2 with respect to damage TS at location L_3.

4.3. Triple damage scenarios

All the single and double damage scenarios assessed in sections 4.2 and 4.3 contain slots with equal depths of 20mm, where the results showed that the proposed damage index has a good capability in detecting damage location. In this section, to assess the capability of the proposed damage index in identifying the damage severity, a total number of 12 triple damage scenarios with different geometric shapes, at different locations of the prestressed concrete slab samples were created. The depth of the slots has been taken variable equal to 5, 10, 20, 30, 40, 50mm, respectively. The notation of T_L_1,T_a_L_2,T_b_L_3,T_c-dr is used for designating the triple damage scenarios, where T is the symbol for the triple damage, L_1, L_2, and L_3 denote the location of damages at the middle and corners of the prestressed concrete slab models, T_a, T_b and T_c demonstrate the type of damage (TS,LS, IS and CS) and dr is the depth ratio and is defined as slot depth to slab thickness ratio which for slots with depths of 5, 10, 20, 30, 40 and 50mm is equal to 5, 10, 20, 30, 40 and 50%, respectively. The numerical models of the prestressed concrete slabs with triple damage scenarios are classified in two groups of T_L_1,TS_L_2,LS_L_3,IS-dr and T_L_1,LS_L_2,CS_L_3,TS-dr, based on the geometric shape of the damages. The corresponding geometric properties and maximum calculated values of the damage index $DI_{i,j}$ per each of them are given in Table 5.

The results of proposed damage index $DI_{i,j}$ for the prestressed concrete slab models with triple damage scenarios in T_L_1,TS_L_2,LS_L_3,IS-dr and T_L_1,LS_L_2,CS_L_3,TS-dr groups are given in Figs. 16 and 17, respectively.

Table 5
Geometric properties and maximum value of damage index $DI_{i,j}$ for triple damage scenarios.

Damage Scenario			Damage Location	Damage Shape	Depth ratio (dr)	Damage Index DI_{ij}
Group	**Name**					
T_L_1,TS_L_2,LS_L_3,IS_dr	T_L_1,TS_L_2,LS_L_3,IS_5%	L_1,TS	L_1	Transverse Slot	5%	0.0553
		L_2,LS	L_2	Longitudinal Slot		0.0032
		L_3,IS	L_3	Inclined Slot		1.4065
	T_L_1,TS_L_2,LS_L_3,IS_10%	L_1,TS	L_1	Transverse Slot	10%	0.1407
		L_2,LS	L_2	Longitudinal Slot		0.0152
		L_3,IS	L_3	Inclined Slot		1.4148
	T_L_1,TS_L_2,LS_L_3,IS_20%	L_1,TS	L_1	Transverse Slot	20%	0.3410
		L_2,LS	L_2	Longitudinal Slot		0.0295
		L_3,IS	L_3	Inclined Slot		1.4389
	T_L_1,TS_L_2,LS_L_3,IS_30%	L_1,TS	L_1	Transverse Slot	30%	0.5070
		L_2,LS	L_2	Longitudinal Slot		0.0307
		L_3,IS	L_3	Inclined Slot		1.4736
	T_L_1,TS_L_2,LS_L_3,IS_40%	L_1,TS	L_1	Transverse Slot	40%	0.5538
		L_2,LS	L_2	Longitudinal Slot		0.0510
		L_3,IS	L_3	Inclined Slot		1.5619
	T_L_1,TS_L_2,LS_L_3,IS_50%	L_1,TS	L_1	Transverse Slot	50%	0.6192
		L_2,LS	L_2	Longitudinal Slot		0.0694
		L_3,IS	L_3	Inclined Slot		1.7671
T_L_1,LS_L_2,CS_L_3,TS_dr	T_L_1,LS_L_2,CS_L_3,TS_5%	L_1,LS	L_1	Longitudinal Slot	5%	0.0126
		L_2,CS	L_2	Curved Slot		0.6700
		L_3,TS	L_3	Transverse Slot		0.0113
	T_L_1,LS_L_2,CS_L_3,TS_10 %	L_1,LS	L_1	Longitudinal Slot	10%	0.0217
		L_2,CS	L_2	Curved Slot		0.7037
		L_3,TS	L_3	Transverse Slot		0.0282
	T_L_1,LS_L_2,CS_L_3,TS_20 %	L_1,LS	L_1	Longitudinal Slot	20%	0.0328
		L_2,CS	L_2	Curved Slot		0.7582
		L_3,TS	L_3	Transverse Slot		0.0770
	T_L_1,LS_L_2,CS_L_3,TS_30 %	L_1,LS	L_1	Longitudinal Slot	30%	0.0349
		L_2,CS	L_2	Curved Slot		0.7739
		L_3,TS	L_3	Transverse Slot		0.1494
	T_L_1,LS_L_2,CS_L_3,TS_40 %	L_1,LS	L_1	Longitudinal Slot	40%	0.0508
		L_2,CS	L_2	Curved Slot		0.7783
		L_3,TS	L_3	Transverse Slot		0.2285
	T_L_1,LS_L_2,CS_L_3,TS_50 %	L_1,LS	L_1	Longitudinal Slot	50%	0.0746
		L_2,CS	L_2	Curved Slot		0.7794
		L_3,TS	L_3	Transverse Slot		0.5031

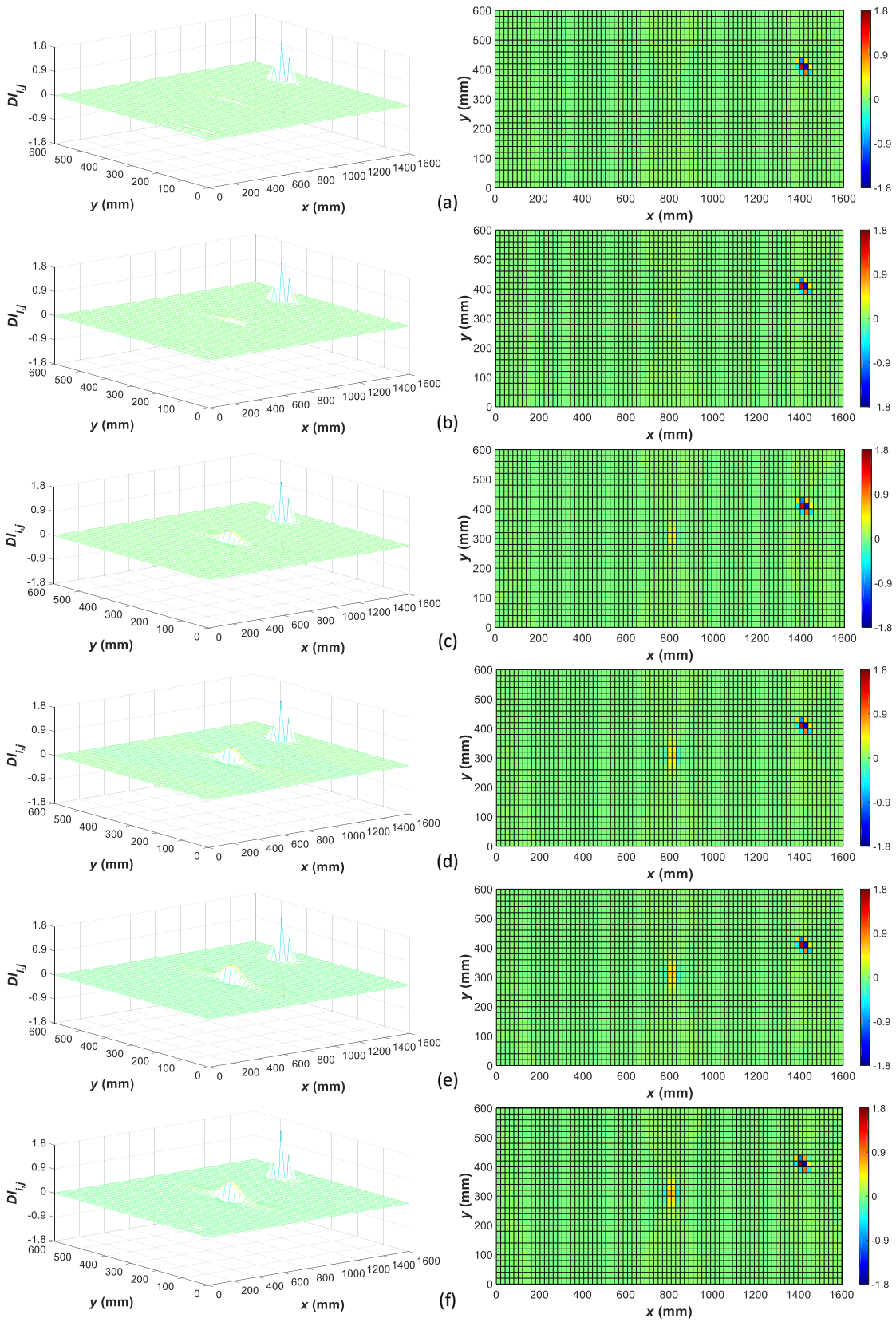

Fig. 16. Triple damage scenarios identification of T_L_1,TS_L_2,LS_L_3,IS-dr group using the damage index $DI_{i,j}$ with different depth ratios (dr): a) 5%; b) 10%; c) 20%; d) 30%; e) 40% and f) 50%

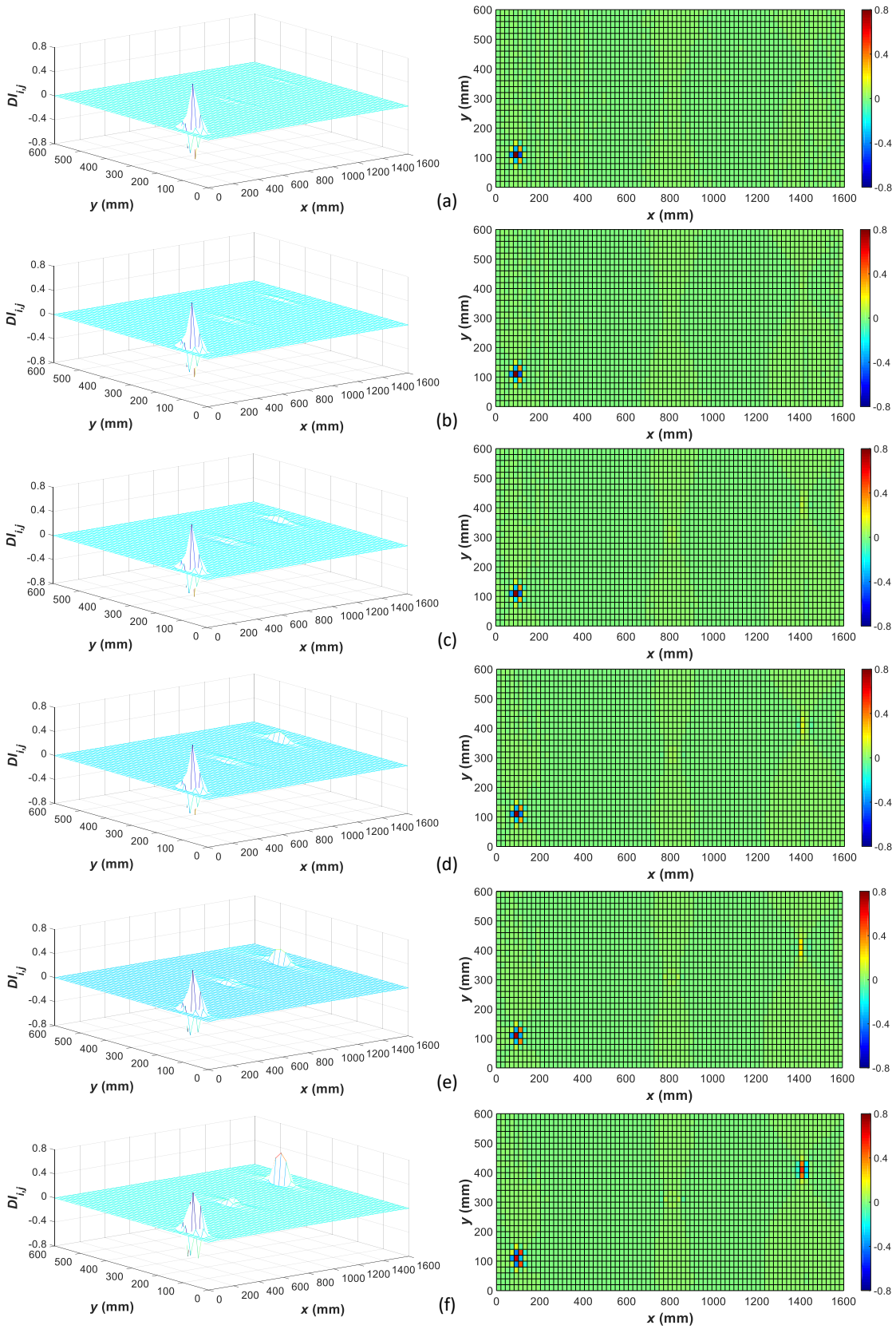

Fig. 17. Triple damage scenarios identification of T_L_1,LS_L_2,CS_L_3,TS-dr group using the damage index $DI_{i,j}$ with different depth ratios (dr): a) 5%; b) 10%; c) 20%; d) 30%; e) 40% and f) 50%.

The results of Table 5 and Fig. 16 show that in general, the damage index $DI_{i,j}$, in addition to detecting the single and double damage scenarios, has been capable of detecting the triple damage scenarios. In accordance with the obtained results in previous sections, in triple damage scenarios, the sensitivity of damage index to damage type IS at location L_3 is higher with respect to damage TS at the middle of prestressed concrete slab models (location L_1), and Damage LS at location L_2. Furthermore, the damage index value has increased with an increase in the depth ratio (dr), from 5% to 50% for all TS, LS, and IS damages at locations L_1, L_2, and L_3. Hence, it could be stated that the proposed damage index, in addition to identifying the location of triple damages, is capable of assessing their severity, too.

The results obtained for damage scenarios of T_L_1,LS_L_2,CS_L_3,TS-dr group in Fig. 17 show that the proposed damage index has a higher sensitivity to damage type CS at location L_2 with respect to LS and TS damages created at locations L_1 and L_3, respectively. Furthermore, the damage index has well identified the triple damage scenarios with different depth ratios (dr) for T_L_1,LS_L_2,CS_L_3,TS-dr group, so that the value of the damage index increases with an increase in the depth ratio corresponding to each prestressed concrete slab model.

5. Discussions

In general, investigating the results of applying the damage index $DI_{i,j}$ on the prestressed concrete slab models with single damage scenarios given in Table 3 and Figs. 10, 11 and 12, show that contrary to the available damage identification methods, the proposed damage index, in addition to the middle locations (L_1 location), has a good ability in identifying each of the single damage scenarios with different geometric shapes of TS, LS, IS and CS at the corners of the slabs (locations L_2 and L_3). Assessing the maximum values of damage index $DI_{i,j}$ of the single damage scenarios given in Table 3 and Fig. 18 show that sensitivity of the damage index in detecting damages with geometric shapes of TS and LS is higher at the middle of the slab (S_L_1,TS, and S_L_1,LS models) with respect to the slab corners (S_L_2,TS, S_L_2,LS, S_L_3,TS and S_L_3,LS models). On the other hand, the damage scenarios with geometric shapes of IS and CS yield higher values of maximum damage index at the slab corners (S_L_2,IS, S_L_2,CS, S_L_3,IS and S_L_3,TS models) than the middle of slab (S_L_1,IS and S_L_1,CS models). As the first mode shape and correspondingly, the first modal curvature of pre-stressed concrete slab is considered as the damage index input, the damage index is more sensitive to damage scenarios in the middle of slab. On the other hand, as Contourlet transform utilizes a diagonal windowing process in processing the input signals, the curved and inclined slots (CS and IS, respectively) resulted more values of proposed damage index.

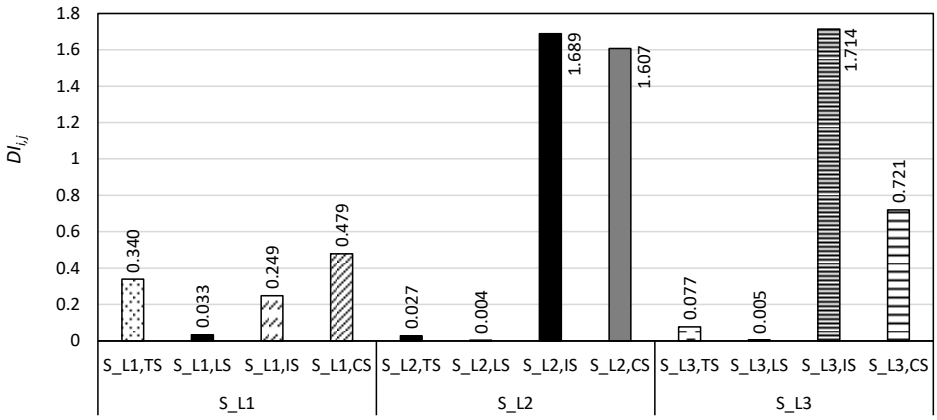

Fig. 18. Maximum values of the damage index $DI_{i,j}$ for single damage scenarios.

Investigating the results of prestressed concrete slab models with double damage scenarios in Table 4 and Figs. 13, 14, and 15 show that the proposed damage index $DI_{i,j}$, in addition to identifying the single damages, is also capable of detecting double damages with different geometric shapes and at different locations. According to Table 4 and Fig. 19, the maximum values of damage index $DI_{i,j}$ for the double damage scenarios show that this index has a higher sensitivity to the occurrence of transverse slot (TS) and longitudinal slots (LS) damages at the middle of the prestressed concrete slab (location L_1) with respect to the corners (locations L_2 and L_3). On the other hand, for the inclined slots (IS) and curved slots (CS), the proposed damage index sensitivity to the corners of the prestressed concrete slab models (locations L_2 and L_3) is higher or equal to its sensitivity to the middle of models (location L_1). Comparison of the obtained results for the damage scenarios with different geometric shapes at identical locations shows that the proposed damage index has the highest sensitivity to damage types of inclined (IS) and curved (CS) slots, respectively, and then, are ranked the damage types of transverse (TS) and longitudinal (LS) slots.

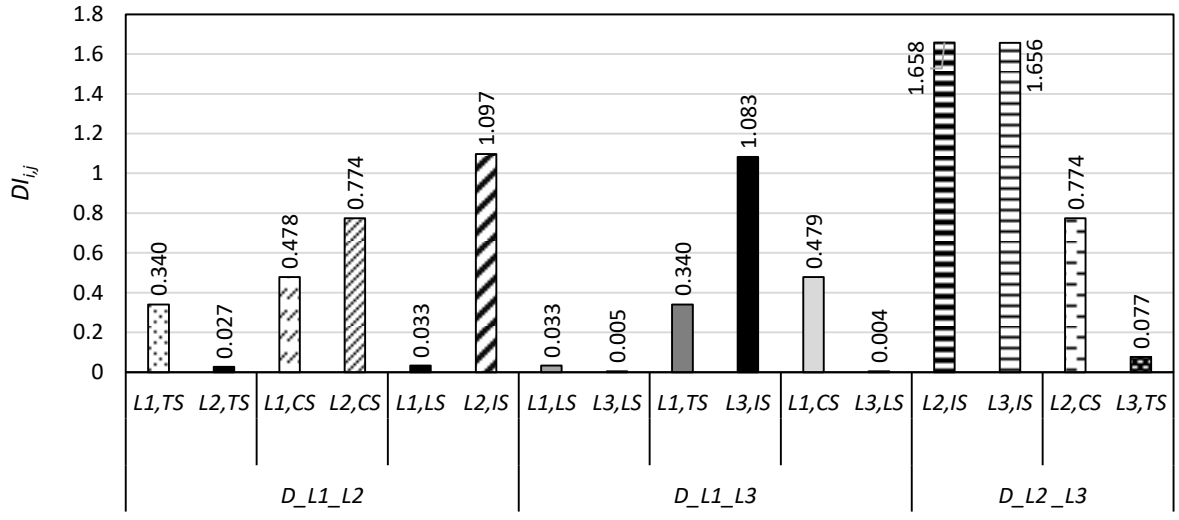

Fig. 19. Maximum values of the damage index $DI_{i,j}$ for double damage scenarios.

In general, investigating Table 5 and Figs. 16 and 17 show that the proposed damage index $DI_{i,j}$, while identifying the single and double damage scenarios, has been capable of identifying the location and severity of triple damage scenarios in prestressed concrete slab models with different geometric shapes and at different locations and different slot depth to slab thickness ratios. The maximum values of damage index $DI_{i,j}$ given in Table 5 and Fig. 20 show that the damage index has the highest sensitivity to damages with geometric shapes of inclined slots (IS), curved slots (CS), Transverse slots (TS), and longitudinal slots (LS), respectively. On the other hand, the sensitivity of damage index to the rate of increase in the depth ratio (dr), increase in the damage severity, is maximum for damage TS at locations L_1 and L_3 and is minimum for damage IS at location L_3 and damage CS at location L_2.

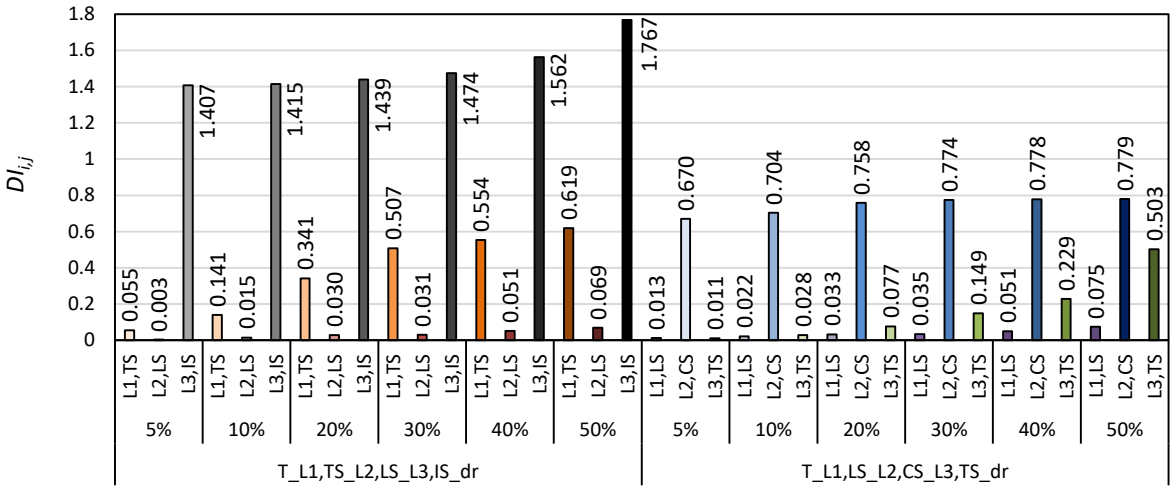

Fig. 20. Maximum values of the damage index $DI_{i,j}$ for triple damage scenarios.

6. Conclusions

In this paper, the contourlet transform, as a novel signal processing method is used for modal data analyzing and assessing the location and severity of damages in the prestressed concrete slab models. For this purpose, first, the numerical models which were built based on the modal testing results which were performed on experimental specimens of prestressed concrete slabs were verified. Then, various cases of damage scenarios at the middle (location L_1) and corners (locations L2 and L3, near to the supports and with a little distance to the supports, respectively) were created in the numerical models. The damages had different geometric shapes of transverse slots (TS), longitudinal slots (LS), inclined slots (IS), with 10mm width and 60mm length and curved slots (CS), with 10mm width and 60mm outer diameter, in the form of single, double and triple damage scenarios. The depth of these slots was taken constant equal to 20mm in the single and double damage scenarios and for assessing damage severity, the depth of the slot in the triple damage scenarios was considered variable with values of 5, 10,20,30,40, and 50mm in the models. By calculating the vibration mode shapes, the contourlet transform coefficients of modal curvatures corresponding to the first mode of prestressed concrete slab models in both damaged and undamaged states were selected as the inputs of the proposed damage index, per each damage scenario. In summary, the following results are obtained:

- The results show that the proposed damage index while identifying the location of single and double damage scenarios, has been able to identify the location and severity of the triple damage scenarios in the prestressed concrete slab models, which had various geometric shapes at different locations and with different severities.
- The maximum values of the presented damage index show that the proposed damage index has the highest sensitivity to damages with geometric shapes of inclined slots (IS), curved slots (CS), transverse slots (TS), and longitudinal slots (LS), respectively.
- Investigation of the maximum values of the proposed damage index for the single damage indices shows that the sensitivity of damage index in detecting damages with geometric shapes of transverse slots (TS) and longitudinal slots (LS) at the middle (location L_1) of slabs is higher than its corners (locations L_1, L_2, and L_3). On the other hand, the single damage scenarios with geometric shapes of inclined slot (IS) and curved slot (CS) have a higher value of maximum damage index at the corners of the slab in comparison to the middle.
- In the double damage scenarios, the proposed damage index has a higher sensitivity to the damage scenarios with geometric shapes of transverse slot (TS) and longitudinal slot (LS) at the middle of the prestressed concrete slabs (location L_1) with respect to the slab corners (locations L_2 and L_3). On the other hand, for damages with geometric shapes of transverse slots (IS) and curved slots (CS), the sensitivity of the proposed damage index at the corners of the prestressed concrete slab samples (locations L_2 and L_3) is higher or equal to its sensitivity at the middle of the sample (location L_1).
- Results of the numerical models of models with triple damage scenarios show that the sensitivity of the proposed damage index to the rate of increase in damage sensitivity (increase in the depth ratio, dr) for damages with geometric shapes of transverse slot (TS) at the corners of the prestressed concrete slab models (locations L_1 and L_3) has the maximum value, While, this value is minimum for damages with the geometric shape of inclined slot (IS) at location L_3 and damages with the geometric shape of curved slot (CS) at location L_2.

Funding

This research received no external funding.

Conflicts of interest

The authors declare no conflict of interest.

References

[1] Yan R, Chen X, Mukhopadhyay SC. Structural Health Monitoring. vol. 26. Cham: Springer International Publishing; 2017. doi:10.1007/978-3-319-56126-4.

[2] Ghalehnovi M, Yousefi M, Karimipour A, de Brito J, Noroozıyan M. Investigation of the Behaviour of Steel-Concrete-Steel Sandwich Slabs with Bi-Directional Corrugated-Strip Connectors. Appl Sci 2020;10:8647. doi:10.3390/app10238647.

[3] Ghalehnovi M, Karimipour A, de Brito J, Chaboki HR. Crack Width and Propagation in Recycled Coarse Aggregate Concrete Beams Reinforced with Steel Fibres. Appl Sci 2020;10:7587. doi:10.3390/app10217587.

[4] Karimipour A, Rakhshanimehr M, Ghalehnovi M, de Brito J. Effect of different fibre types on the structural performance of recycled aggregate concrete beams with spliced bars. J Build Eng 2021;38:102090. doi:10.1016/j.jobe.2020.102090.

[5] Karimipour A, de Brito J. Influence of polypropylene fibres and silica fume on the mechanical and fracture properties of ultra-high-performance geopolymer concrete. Constr Build Mater 2021;283:122753. doi:10.1016/j.conbuildmat.2021.122753.

[6] Rezaiee-Pajand M, Karimipour A, Abad JMN. Crack Spacing Prediction of Fibre-Reinforced Concrete Beams with Lap-Spliced Bars by Machine Learning Models. Iran J Sci Technol Trans Civ Eng 2020. doi:10.1007/s40996-020-00441-6.

[7] Jahangir H, Bagheri M. Evaluation of Seismic Response of Concrete Structures Reinforced by Shape Memory Alloys (Technical Note). Int J Eng 2020;33. doi:10.5829/ije.2020.33.03c.05.

[8] Jahangir H, Bagheri M, Delavari SMJ. Cyclic Behavior Assessment of Steel Bar Hysteretic Dampers Using Multiple Nonlinear Regression Approach. Iran J Sci Technol Trans Civ Eng 2020. doi:10.1007/s40996-020-00497-4.

[9] Santandrea M, Imohamed IAO, Jahangir H, Carloni C, Mazzotti C, De Miranda S, et al. An investigation of the debonding mechanism in steel FRP- and FRCM-concrete joints. 4th Work New Boundaries Struct Concr, Capri Island, Italy: 2016, p. 289–98.

[10] Jahangir H, Esfahani MR. Numerical Study of Bond – Slip Mechanism in Advanced Externally Bonded Strengthening Composites. KSCE J Civ Eng 2018;22:4509–18. doi:10.1007/s12205-018-1662-6.

[11] Jahangir H, Esfahani MR. Strain of Newly – Developed Composites Relationship in Flexural Tests (In Persian). J Struct Constr Eng 2018;5:92–107. doi:10.22065/jsce.2017.91828.1255.

[12] Bagheri M, Chahkandi A, Jahangir H. Seismic Reliability Analysis of RC Frames Rehabilitated by Glass Fiber-Reinforced Polymers. Int J Civ Eng 2019. doi:10.1007/s40999-019-00438-x.

[13] Jahangir H, Esfahani MR. Investigating loading rate and fibre densities influence on SRG - concrete bond behaviour. Steel Compos Struct 2020;34:877–89. doi:10.12989/scs.2020.34.6.877.

[14] Jahangir H, Esfahani MR. Experimental analysis on tensile strengthening properties of steel and glass fiber reinforced inorganic matrix composites. Sci Iran 2020. doi:10.24200/SCI.2020.54787.3921.

[15] Seyedpoor SM, Ahmadi A, Pahnabi N. Structural damage detection using time domain responses and an optimization method. Inverse Probl Sci Eng 2019;27:669–88. doi:10.1080/17415977.2018.1505884.

[16] Rezazadeh Eidgahee D, Haddad A, Naderpour H. Evaluation of shear strength parameters of granulated waste rubber using artificial neural networks and group method of data handling. Sci Iran 2019;26:3233–44. doi:10.24200/sci.2018.5663.1408.

[17] Naderpour H, Rezazadeh Eidgahee D, Fakharian P, Rafiean AH, Kalantari SM. A new proposed approach for moment capacity estimation of ferrocement members using Group Method of Data Handling. Eng Sci Technol an Int J 2020;23:382–91. doi:10.1016/j.jestch.2019.05.013.

[18] Rezazadeh Eidgahee D, Rafiean AH, Haddad A. A Novel Formulation for the Compressive Strength of IBP-Based Geopolymer Stabilized Clayey Soils Using ANN and GMDH-NN Approaches. Iran J Sci Technol Trans Civ Eng 2019. doi:10.1007/s40996-019-00263-1.

[19] Jahangir H, Rezazadeh Eidgahee D. A new and robust hybrid artificial bee colony algorithm – ANN model for FRP-concrete bond strength evaluation. Compos Struct 2021;257:113160. doi:10.1016/j.compstruct.2020.113160.

[20] Heidari A, Raeisi J. Optimum design of structures against earthquake by simulated annealing using wavelet transform. J Soft Comput Civ Eng 2018;2:23–33. doi:10.22115/SCCE.2018.125682.1055.

[21] Naderpour H, Fakharian P. A synthesis of peak picking method and wavelet packet transform for structural modal identification. KSCE J Civ Eng 2016;20:2859–67. doi:10.1007/s12205-016-0523-4.

[22] Jahangir H, Esfahani MR. Structural Damage Identification Based on Modal Data and Wavelet Analysis. 3rd Natl Conf Earthq Struct, Kerman, Iran: 2012.

[23] Shah M, Mevada S, of VP-IJ, 2016 undefined. Comparative Study of Diagrid Structures with Conventional Frame Structures. IngentaconnectCom n.d.

[24] Jiang T, Kong Q, Patil D, Luo Z, Huo L, Song G. Detection of Debonding Between Fiber Reinforced Polymer Bar and Concrete Structure Using Piezoceramic Transducers and Wavelet Packet Analysis. IEEE Sens J 2017;17:1992–8. doi:10.1109/JSEN.2017.2660301.

[25] Qu H, Li T, Chen G. Adaptive wavelet transform: Definition, parameter optimization algorithms, and application for concrete delamination detection from impact echo responses. Struct Heal Monit 2018:147592171877620. doi:10.1177/1475921718776200.

[26] Naito H, Bolander JE. Damage detection method for RC members using local vibration testing. Eng Struct 2019;178:361–74. doi:10.1016/j.engstruct.2018.10.031.

[27] Mokhtari Masinaei M, Jahangir H, Khatibinia M. Damage Detection in Prestressed Concrete Slabs Using Vibrational Responses in Time Domain. 5th Natl Conf Recent Adv Civ Eng Archit Urban Dev, Shahid Beheshti University, Tehran, Iran: 2019.

[28] Jahangir H, Esfahani MR. Assessment of structural damage severity using the energy due to dynamic response (In Persian). 2nd Int Conf Acoust Vib, Tehran, Iran: 2012.

[29] Pahlevan Mosavari, A. Jahangir H, Esfahani MR. The Effect of Sensor Weight on Obtained Data from Modal Tests (In Persian). 9th Natl Congr Civ Eng, Mashhad, Iran: Ferdowsi University of Mashhad; 2016.

[30] Moughty JJ, Casas JR. A State of the Art Review of Modal-Based Damage Detection in Bridges: Development, Challenges, and Solutions. Appl Sci 2017;7:510. doi:10.3390/app7050510.

[31] Yang YB, Yang JP. State-of-the-Art Review on Modal Identification and Damage Detection of Bridges by Moving Test Vehicles. Int J Struct Stab Dyn 2018;18:1850025. doi:10.1142/S0219455418500256.

[32] Wang S, Xu M. Modal Strain Energy-based Structural Damage Identification: A Review and Comparative Study. Struct Eng Int 2019;29:234–48. doi:10.1080/10168664.2018.1507607.

[33] Jahangir H, Daneshvar Khoram MH, Esfahani MR. Application of vibration modal data in gradually detecting structural damage (In Persian). 4th Int Conf Acoust Vib, Tehran, Iran: 2014.

[34] Seyedi SR, Keyhani A, Jahangir H. An Energy-Based Damage Detection Algorithm Based on Modal Data. 7th Int Conf Seismol Earthq Eng, International Institute of Earthquake Engineering and Seismology (IIEES); 2015, p. 335–6.

[35] Daneshvar MH, Gharighoran A, Zareei SA, Karamodin A. Damage Detection of Bridge by Rayleigh-Ritz Method. J Rehabil Civ Eng 2020;8:111–20. doi:10.22075/JRCE.2019.17603.1337.

[36] Do MN, Vetterli M. Contourlets: a directional multiresolution image representation. Proceedings Int Conf Image Process, vol. 1, IEEE; 2002, p. I-357-I–360. doi:10.1109/ICIP.2002.1038034.

[37] Shahrokhinasab E, Hosseinzadeh N, Monirabbasi A, Torkaman S. Performance of Image-Based Crack Detection Systems in Concrete Structures. J Soft Comput Civ Eng 2020;4:127–39. doi:10.22115/SCCE.2020.218984.1174.

[38] Ma C-X, Zhao C-X, Hou Y. Pavement Distress Detection Based on Nonsubsampled Contourlet Transform. 2008 Int Conf Comput Sci Softw Eng, IEEE; 2008, p. 28–31. doi:10.1109/CSSE.2008.1027.

[39] Zhibiao S, Yanqing G. Algorithm on Contourlet Domain in Detection of Road Cracks for Pavement Images. J Algorithm Comput Technol 2013;7:15–25. doi:10.1260/1748-3018.7.1.15.

[40] Fan Y. A Pavement Cracks Detection Algorithm Based on NSCT Domain. J Inf Comput Sci 2015;12:4791–8. doi:10.12733/jics20106356.

[41] Qian Q, Dang Q, Zhao C, He J. Recognition of pavement damage types based on features fusion. 2018 Tenth Int Conf Adv Comput Intell, IEEE; 2018, p. 239–42. doi:10.1109/ICACI.2018.8377613.

[42] Ai Y, Xu K. Feature extraction based on contourlet transform and its application to surface inspection of metals. Opt Eng 2012;51:113605. doi:10.1117/1.OE.51.11.113605.

[43] Hajizadeh AR, Salajegheh J, Salajegheh E. Performance evaluation of wavelet and curvelet transforms based-damage detection of defect types in plate structures. Struct Eng Mech 2016;60:667–91. doi:10.12989/sem.2016.60.4.667.

[44] Li J, Cao B, Nie F, Zhu M. Feature Extraction of Foam Nickel Surface Based on Multi-Scale Texture Analysis. J Adv Comput Intell Intell Informatics 2019;23:175–82. doi:10.20965/jaciii.2019.p0175.

[45] Vafaie S, Salajegheh E. Comparisons of wavelets and contourlets for vibration-based damage identification in the plate structures. Adv Struct Eng 2019;22:1672–84. doi:10.1177/1369433218824903.

[46] Mallat S. A wavelet tour of signal processing. London, UK: Academic Press; 1999.

[47] Burt P, Adelson E. The Laplacian Pyramid as a Compact Image Code. IEEE Trans Commun 1983;31:532–40. doi:10.1109/TCOM.1983.1095851.

[48] Bamberger RH, Smith MJT. A filter bank for the directional decomposition of images: theory and design. IEEE Trans Signal Process 1992;40:882–93. doi:10.1109/78.127960.

[49] Po DD-Y, Do MN. Directional multiscale modeling of images using the contourlet transform. IEEE Trans Image Process 2006;15:1610–20. doi:10.1109/TIP.2006.873450.

[50] Do MN, Vetterli M. The contourlet transform: an efficient directional multiresolution image representation. IEEE Trans Image Process 2005;14:2091–106. doi:10.1109/TIP.2005.859376.

[51] Pahlevan Mosavari M. Damage detection on slabs using modal analysis. Ferdowsi University of Mashhad, 2014.

[52] Lubliner J, Oliver J, Oller S, Oñate E. A plastic-damage model for concrete. Int J Solids Struct 1989;25:299–326. doi:10.1016/0020-7683(89)90050-4.

[53] Oñate E, Oller S, Oliver J, Lubliner J. A constitutive model for cracking of concrete based on the incremental theory of plasticity. Eng Comput 1988;5:309–19. doi:10.1108/eb023750.

[54] Oller S, Oñate E, Miquel J, Botello S. A plastic damage constitutive model for composite materials. Int J Solids Struct 1996;33:2501–18. doi:10.1016/0020-7683(95)00161-1.

[55] Pandey AK, Biswas M, Samman MM. Damage detection from changes in curvature mode shapes. J Sound Vib 1991;145:321–32. doi:10.1016/0022-460X(91)90595-B.

[56] Qiao P, Lu K, Lestari W, Wang J. Curvature mode shape-based damage detection in composite laminated plates. Compos Struct 2007;80:409–28. doi:10.1016/j.compstruct.2006.05.026.